

## **UC Santa Cruz**

### **UC Santa Cruz Electronic Theses and Dissertations**

#### **Title**

Creating CZTS Thin Films Via Stacked Metallic CVD and Sulfurization

#### **Permalink**

<https://escholarship.org/uc/item/3z2043fd>

#### **Author**

Bielecki, Anthony

#### **Publication Date**

2013

Peer reviewed|Thesis/dissertation

UNIVERSITY OF CALIFORNIA

SANTA CRUZ

**CREATING CZTS THIN FILMS VIA STACKED METALLIC CVD  
AND SULFURIZATION**

A thesis submitted in partial satisfaction  
of the requirements for the degree of

MASTER OF SCIENCE

in

PHYSICS

by

**Anthony Bielecki**

September 2013

The Thesis of Anthony Bielecki  
is approved:

---

Professor Sue Carter, Chair

---

Professor David Smith

---

Professor Joshua Deutsch

---

Tyrus Miller  
Vice Provost and Dean of Graduate Studies

Copyright © by  
Anthony Bielecki  
2013

# Table of Contents

List of Figures . . . . .	v
List of Tables . . . . .	vii
Abstract . . . . .	viii
Dedication . . . . .	ix
<b>1 Introduction</b>	<b>1</b>
1.1 Thin-Film Photovoltaics . . . . .	1
1.2 Copper Indium Galenide Films . . . . .	2
1.3 CZTS Thin Films . . . . .	2
<b>2 Experimental Methods</b>	<b>5</b>
2.1 Ampoules . . . . .	5
2.2 Valves & Programming . . . . .	6
2.3 Deposition Chamber . . . . .	7
2.4 Substrates . . . . .	7
<b>3 Deposition Characterization Techniques &amp; Results</b>	<b>9</b>
3.1 Determining Thickness & Growth Rate By Atomic Force Microscopy	10
3.2 Ultraviolet-visible-infrared Spectroscopy . . . . .	12
3.3 Energy-Dispersive X-Ray Spectroscopy . . . . .	13
3.4 X-Ray Diffraction . . . . .	14
3.5 Four-Point Resistivity . . . . .	16
<b>4 Discussion</b>	<b>18</b>

<b>5 Conclusion</b>	<b>20</b>
5.1 Test Figure/Table . . . . .	21
<b>Appendices</b>	<b>22</b>

# List of Figures

1	Step-height histogram for AFM scan of scratched CTZ-1 film. . . . .	23
2	Step-height histogram for AFM scan of scratched CTZ-2 film. . . . .	23
3	Step-height histogram for AFM scan of scratched ZTC-1 film. . . . .	24
4	Step-height histogram for AFM scan of scratched TCZ-1 film. . . . .	24
5	Step-height histogram for AFM scan of scratched TCZ-2 film. . . . .	25
6	Step-height histogram for AFM scan of scratched CZT-1 film. . . . .	25
7	Relative height histogram for surface scan of CTZ-1. . . . .	26
8	Relative height histogram for AFM surface scan of CTZ-2. . . . .	26
9	Relative height histogram for AFM surface scan of ZTC-1. . . . .	27
10	Relative height histogram for AFM surface scan of TCZ-1. . . . .	27
11	Relative height histogram for AFM surface scan of TCZ-2. . . . .	28
12	Relative height histogram for AFM surface scan of CZT-1. . . . .	28
13	Tauc plot for CTZ-1. The fit line intercepts the x-axis at 3.40 eV. .	28
14	Tauc plot for CTZ-2. The fit line intercepts the x-axis at 1.63 eV. .	29
15	Tauc plot for TCZ-1. The fit line intercepts the x-axis at 2.02 eV. .	29
16	Tauc plot for TCZ-2. The fit line intercepts the x-axis at 2.39 eV. .	29
17	Tauc plot for CZT-1. The fit line intercepts the x-axis at 1.87 eV. .	30
18	Tauc plot for ZTC-1. The fit line intercepts the x-axis at 1.08 eV. .	30
19	EDX spectrum for CTZ-1 at 1000X magnification. . . . .	31
20	EDX spectrum for CTZ-2 at 1000X magnification. . . . .	31
21	EDX spectrum for ZTC-1 at 1000X magnification. . . . .	31
22	EDX spectrum for TCZ-1 at 1000X magnification. . . . .	31
23	EDX spectrum for TCZ-2 at 1000X magnification. . . . .	31

24	EDX spectrum for CZT-1 at 1000X magnification. . . . .	32
25	X-ray diffraction pattern for CTZ-1 showing intensity (y-axis) versus diffraction angle (x-axis). . . . .	32
26	X-ray diffraction pattern for CTZ-2. . . . .	32
27	X-ray diffraction pattern for CZT-1. . . . .	32
28	X-ray diffraction pattern for TCZ-1. . . . .	32
29	X-ray diffraction pattern for TCZ-2. . . . .	33
30	: Reference XRD pattern for three different stacking orders of CZTS. Stacked type A corresponds to CTZ, B to ZCT, and C to TZC. (This image is taken from reference 17) . . . . .	33
31	Effective circuit for 4-point resistivity measurement. $R_{Ci}$ is the resis- tance due to contact $i$ , $R_S$ is the resistance of the sample, $R_M$ is the equivalent resistance of the voltmeter, $V_S$ is the voltage across the sample, and $V_M$ is the voltage measured using the voltmeter. . . . .	33

# List of Tables

1	Atomic Force Microscopy Data . . . . .	34
2	Direct Band Gaps . . . . .	34
3	Stoichiometric Ratios . . . . .	34
4	Summary results of EDX spectrum for CTZ-1 at 1000X magnification	34
5	Summary results of EDX spectrum for CTZ-2 at 1000X magnification	34
6	Summary results of EDX spectrum for ZTC-1 at 1000X magnification	35
7	Summary results of EDX spectrum for TCZ-1 at 1000X magnification	35
8	Summary results of EDX spectrum for TCZ-2 at 1000X magnification	35
9	Summary results of EDX spectrum for CZT-1 at 1000X magnification	35
10	Four-Point Resistivity Measurements . . . . .	35

## Abstract

### CREATING CZTS THIN FILMS VIA STACKED METALLIC CVD AND SULFURIZATION

by

Anthony Bielecki

$\text{Cu}_2\text{ZnSnS}_4$  (CZTS) thin film photovoltaics is an increasingly important area of research for solar energy due to the high abundance and low toxicity of the elements used. A series of chemical vapor depositions (CVDs) with copper, tin, and zinc precursors were carried out to create layered thin films on quartz substrates. The viability of creating CZTS using these precursors was examined. As far as the author is aware, no work has yet been published on creating CZTS using the particular tin precursor that was used here, Dibutyltin Diacetate. Four different precursor stacking sequences were examined. Depositions were characterized using atomic force microscopy, energy-dispersive x-ray spectroscopy, x-ray diffraction, and four-point resistivity measurements. It was found that the ordering of precursors has a significant effect on the properties of the resulting thin films. The band gap energies were found to range from 1.08 eV to 2.02 eV.

The challenge of writing a dedication is that you only get one and its easy to spread it too thin. I have to thank my professors of course. And Id feel terrible not thanking my parents seeing as how they covered tuition, not to mention the whole feeding-and-raising me thing. My friends have proofread my work so they should be thanked too. And, while Im at it, I might as well thank the 7-11 clerk who sold me those RedBulls on late nights when I had to pry my eyes open with caffeine to crank out another few pages. The list of people Im irrevocably indebted to goes on and on. I might as well staple a phone book to this dedication page. So, as to not delude the thank you too much, and with apologies to those not included, I hereby dedicate this work to two, and only two, people: Professor Joshua Deutsch and Professor William Saxton. They gave me my start. Without them I never could have been involved in this project. Its one of lifes damn shames that the people who affect you for the better rarely know the extent of their impact. Mulling over a physics problem at 3 AM, I might consider how my mentors would approach it, draw strength in the face of utter confusion from the example theyve set by their intelligence and dedication, and, asleep in their own beds (or perhaps up late tackling their own problems with the ghosts of their own mentors), they will never know the help theyve given me.

Thank you.

# Chapter 1

## Introduction

### 1.1 Thin-Film Photovoltaics

The term thin film describes a layer of material with a thickness ranging from a fraction of a nanometer (such as a monolayer of molecules) to several micrometers. Electronic semiconductor devices are one of the main applications of thin films because thin film technology has the potential to dramatically reduce to the cost of photovoltaic systems (such as solar cells) due to lower material, energy, and handling costs [1]. Familiar to the general public as the small strips which power hand-held calculators, thin-film photovoltaics (TFPVs) are currently available in large modules (useful as building-integrated installations and vehicle charging systems) and the industry expected to continue growing [1]. It is anticipated that advances in TFPV technology will make them a strong contender for the long sought grid parity objective [1]. Grid parity occurs when an alternative energy source can generate electricity at a cost less than or equal to the price of purchasing power from the electricity grid. Solar cells already offer a number of advantages to current major energy sources such as coal and nuclear power. Scalability and localized installation (which minimizes energy loss due to long-distance transmission) of solar cells means that achieving grid parity will make TFPVs very competitive with other major energy sources.

## 1.2 Copper Indium Galenide Films

Thin-film solar cells are created by depositing layers of photovoltaic material on a substrate. This can be done in a variety of ways. A common method is chemical vapor deposition (CVD), which was used in the experiment and is discussed in more detail in the Section 1.3. There are many photovoltaic materials available for creating thin films; among the more commonly used is copper indium gallium selenide (CIGS). The absorption coefficient of CIGS is unusually high, more than  $10^5 \text{ cm}^{-1}$  for 1.5 eV and higher energy photons [2], making it an excellent candidate for thin-film solar cells. CIGS solar cell efficiencies have been reported near 20%, the current record for any thin film solar cell [3]. However, use of CIGS has a number of drawbacks as well, chief among them are the scarcity and relatively high toxicity of some of the necessary elements [4, 5]. Therefore, alternatives to CIGS have been sought. A mixture of copper, zinc, tin and sulfur,  $\text{Cu}_2\text{ZnSnS}_4$ , more commonly known as CZTS, is one of the most promising alternatives, and the study of this paper.

## 1.3 CZTS Thin Films

CZTS has optical and electronic properties similar to CIGS, making it a favorable choice for thin-film solar cells. CZTS has a direct band gap of 1.5 eV and an absorption coefficient greater than  $10^4 \text{ cm}^{-1}$  in the visible region [5]. Unlike CIGS, CZTS is composed only of abundant and relatively non-toxic elements [6]. It uses sulfur instead of the commonly used, more toxic selenium [5]. There are economic benefits to using CZTS as well. The raw materials needed are roughly five times less expensive than CIGS and it is estimated that there are enough reserves (for Cu, Sn, Zn and S) that the world could be powered with only 0.1% of the available raw material resources [4].

At the time of this writing, the greatest conversion efficiency for a CZTS thin film solar cell is 9.66%, achieved by Todorov et al. [7]. However, photon balance cal-

culations predict that it is theoretically possible to achieve efficiencies as high as 32.2% with CZTS based thin film solar cells [8]. This indicates that further study is needed of different CZTS fabrication methods and viable precursors. Specifically, the effect of fabrication method upon the molecular structure of CZTS should be examined. CZTS can have a structure resembling either kesterite or stannite and can be highly crystalline or amorphous depending on the fabrication method [6]. The author is unaware of any study which compares the efficiencies of CZTS solar cells where the only difference between cells is the level of crystallinity. For this experiment, chemical vapor deposition was used to attempt making CZTS thin film depositions. CVD is a method often used for producing high-purity thin films. A substrate is exposed to precursors in the gaseous phase which deposit on the substrate surface or previous deposition layers. Volatile by-products are often produced in the process, so CVDs must take place under vacuum with a nonreactive gas used to help flush the byproducts. This causes some precursor to be flushed as well so it is critical that the vapor pressure of the precursor entering the chamber be suitably high so that there is enough precursor to coat the substrate.

There are two ways of using CVD to create CZTS; all precursors can be simultaneously deposited or multiple depositions can be made thereby creating different layers of precursors. The latter approach was used in this experiment because it has the advantage that the compositional ratio of the CZTS film can be adjusted relatively easily by altering the thickness of the various layers. The stacking method is also conceivably suitable for industrial scale production and can be adapted to non-vacuum deposition methods if needed [9]. The order in which the precursors are deposited has been shown to have a dramatic effect on the characteristics of the CZTS films [10, 11]. In this experiment, four different precursor orderings were deposited and characterized. These depositions made were Cu/Sn/Zn, Cu/Zn/Sn, Sn/Cu/Zn, & Zn/Sn/Cu, where the first element named was the first deposited and so forth. Sulfur is used in tandem with all metallic precursors so it is not denoted. Hereafter, these combinations will be referred to as CTZ, CZT, TCZ, & ZTC respec-

tively. Determining the characteristics of the remaining two orderings and actually creating CZTS thin-film solar cells will be the focus of future work. To make a solar cell, instead of depositing on blank quartz slides, a glass substrate with patterned indium tin oxide (ITO) would be used. Indium tin oxide is an electrically conductive and transparent oxide useful for attaching electrodes to the solar cell. Nanoparticle titanium oxide must then be spin-coated atop the ITO. Sintering this creates a nanoporous substrate which is suitable for depositing CZTS. Atomic layer deposition (known as ALD, a more controlled type of CVD) would then be used to create CZTS. Finally, gold or silver would be evaporated onto the CZTS, creating a basic solar cell.

In this paper, the properties of thin films, created using different layerings of copper, zinc, and tin precursors, are examined with an eye toward future production of CZTS thin film solar cells. The experimental apparatus and methods used are explained in Section 2. The various analysis techniques needed to characterize the films are detailed in Section 3, along with the corresponding results of the techniques. Section 4 gives a summary of the results and conclusion. All figures and tables can be found in Section 5 and references in Section 6.

## Chapter 2

# Experimental Methods

CVDs were performed using a custom-built deposition system, consisting of a hot-wall tube furnace, quartz deposition tube, ampoules housing the precursors, and a network of stainless steel pipes and valves. The pipes were wrapped in heating cord and aluminum foil for insulation. This helped to prevent precursors from depositing inside of them. The system was kept under vacuum with a base pressure of 10-20 mTorr. During depositions, the pressure was kept below 2 Torr. Nitrogen was used as a carrier and purge gas.

All CVDs were carried out for 30 minutes, during which the total pressure of metal precursor and hydrogen sulfide in the deposition chamber was maintained at approximately 1 torr. After all three CVDs had been performed, the thin film was then annealed in hydrogen sulfide for 30 minutes at 450 C. Four precursor orderings were created, CTZ, CZT, TCZ, and ZTC.

Below, we discuss the individual components of the system in greater detail.

### 2.1 Ampoules

Our system separately houses zinc, copper, and tin precursors in solid form in ampoules. These precursors are highly reactive with oxygen in the atmosphere. There-

fore, the system must be kept under vacuum at all times. The ampoules were wrapped in heating cord so that the precursors can be raised to an appropriate temperature to cause sublimation. The optimum temperature for each precursor ampoule, determined by trial and error, was found to be 55 C for tin, 90 C for copper, and 120 C for zinc. Gaseous precursor was moved to the deposition chamber using nitrogen as a carrier gas. Timing of precursor flow through the system was controlled by pneumatically-actuated valves. At all times, the ampoules must contain only their respective precursor and nitrogen (or some other inert gas) or else the precursor will degrade, causing depositions to be poor or entirely unsuccessful.

Hydrogen Sulfide ( $\text{H}_2\text{S}$ ) was created in situ for each deposition using 0.5 g of aluminum sulfide powder and 50 ml of water. The chemical reaction is  $\text{Al}_2\text{S}_3 + 3\text{H}_2\text{O} \rightarrow \text{Al}_2\text{O}_3 + 3\text{H}_2\text{S}$ . This reaction took place in an ampoule which had flushed of atmosphere by placing it under vacuum to achieve a pressure of 200 mTorr, filling with nitrogen to atmospheric pressure, and repeating for a total of three times. Once the  $\text{H}_2\text{S}$  reaction was completed (resulting in a partial pressure of 400 mmHg), the ampoule was filled with nitrogen to atmospheric pressure. On its way through the system to the deposition chamber, the  $\text{H}_2\text{S}$  was passed through a powder desiccant to reduce the residual water content. Measurements using a residual gas analyzer showed this resulted in a water content of less than 1% in the  $\text{H}_2\text{S}$ .

## 2.2 Valves & Programming

The flow of precursors was governed by computer-controlled valves which regulated which parts of the system received nitrogen flow or were put under vacuum. The timing of the valves and rate of nitrogen flow was orchestrated using a computer program written in C, which controlled the system using mass flow controllers (MFCs). This assured uniform timing for each deposition.

The Hydrogen Sulfide feedthrough line was the only line not entirely controlled

by the computer during CVDs. Unlike the other precursors, which have relatively constant partial pressures throughout the deposition, the pressure in the H<sub>2</sub>S ampoule decreases steadily and dramatically throughout the course of the deposition. Therefore, the flow of H<sub>2</sub>S could be manually adjusted using a needle valve to help maintain constant pressure throughout the depositions.

## 2.3 Deposition Chamber

The deposition chamber consists of a quartz tube enclosed by a tube-furnace. Precursors enter the tube by from feed-through lines located on one side of the tube. The opposing side is connected to the vacuum pump. The chamber must be kept under constant vacuum during depositions to prevent any contamination from the atmosphere. Optimal tube furnace temperature depended on the precursor being used. The tube furnace was heated to 350 C for tin, 200 C for copper, and 150 C for zinc. These temperatures are noticeably higher than the temperatures of the ampoules and feed-through lines. This is because, before the precursors reach the tube furnace, they only need to be heated enough to vaporize. The precursors are all metal-organic compounds, causing them to vaporize at temperatures much lower that would be necessary for pure metals. Once the precursors reach the tube furnace, they must be further heated so that the metals dissociate from the organic components of the compound. If the ampoules and feed-through lines were raised to too high of a temperature, the feed-through lines would get coated in metal and eventually clog.

## 2.4 Substrates

Depositions were made on 1 mm thick, 1 square inch quartz glass slides. These slides were first cleaned by 30 minutes of sonication in ethanol and dried using pressurized nitrogen. The slides fit into the deposition tube such that both faces are exposed

and only the corners touch the tube.

A significant temperature gradient exists within the quartz tube due to the openings in the tube furnace for the feed-throughs and vacuum pump. This causes different growth rates depending on slide placement within the tube. Placing slides approximately 10 cm from the feed-throughs proved optimal, but the exact distance varied depending upon the precursor being used. For each deposition, three slides were placed within the deposition tube. Any slides which showed a significant amount of deposition were analyzed. The labeling system used to differentiate between slides from the same series of depositions is discussed in the next section.

## Chapter 3

# Deposition Characterization

## Techniques & Results

Thin films are typically characterized by determining the film thickness, resistance, band gap, stoichiometry, and, ideally, bond length and structure. It is also often desirable to know the growth rate, which is a property of the deposition method and precursors used. Determining these characteristics requires a range of techniques and measurements which are detailed below.

In all, depositions were successful on six slides, which we call CTZ-1, CTZ-2, TCZ-1, TCZ-2, CZT-1 and ZTC-1. The three letters give the order of precursors from first to last (i.e. CTZ means copper, then tin, then zinc). The number after the letters denotes where the slide was placed within the tube furnace, with lower numbers being closer to the precursor feed-throughs. For example, CTZ-1 and CTZ-2 both underwent the same series of depositions (at the same time) but CTZ-1 was closer to the feed-throughs than CTZ-2. The results for these depositions are also presented below. For the combinations CZT and ZTC, it appears that the slide must be placed in close proximity to the precursor feed-throughs because the slides in the CZT-2 and ZTC-2 positions remained blank.

### 3.1 Determining Thickness & Growth Rate By Atomic Force Microscopy

The basic underlying concepts of atomic force microscopy (AMF) are surprisingly simple. An atomic force microscope makes measurements using a sharp probe tip (typically with a radius of curvature is on the order of nanometers) attached to the end of a cantilever which scans the surface of the sample. It is not necessary for the tip to actually make contact with the surface. Indeed, it is often preferable if it does not since contact can damage the sample and the probe tip. When operated in non-contact mode, the cantilever is made to oscillate at or near its resonant frequency and the probe tip is brought to within a few nanometers of the sample surface. Van der Waals forces between the tip and the sample will cause small deflections in the cantilever in accordance with Hookes Law. By measuring the change in the frequency of the cantilever oscillation, it is possible to deduce the distance between the tip and the samples surface. Scanning over the surface and measuring the tip-to-sample distance at each point allows software to construct a topographic map of the surface.

To measure thin-film thickness of the depositions, they were first scored using a razorblade. This easily cuts through the thin film but does not significantly scratch the underlying quartz. An AFM scan, spanning the surface and the scratch, was performed for each deposition. The resulting image was used to determine the height difference between the surface of the film and the surface of the quartz slide substrate. Since the duration of each CVD was known (30 minutes), once the film thickness was determined it was simple to deduce an average growth rate.

For a given CZTS slide, a 40x40 micrometer area, spanning the score left by the razor, was scanned. To determine an average film thickness, height differentials were averaged from histograms of each scan. To ensure that measurements from the bottom of the scratch didnt lower the calculation for the film thickness, only height differentials greater than 500 nm were considered in the average. Results from previ-

ous experiments have shown that a single thirty-minute CVD with these precursors usually creates a film thickness of approximately 500 - 800 nm [12, 13]. Given that three successive CVDs were used for each film created in this experiment, it is reasonable to assume that any measurement less than 500 nm is the result of imperfect scoring from the razorblade. Histograms of the height differentials from the AFM images taken along scratches in the films are shown in Figures 1 - 6. The average thickness for each slide and growth rates are shown in Table 1. It was found that, among the slides, the thickness ranged from as low as  $704.4 \pm 113.9\text{nm}$  for ZTC-1 to as much as  $1523.0 \pm 501.3\text{nm}$  for CTZ-1, corresponding a range of growth rates from  $7.82 \pm 1.27 \text{ nm / minute}$  to  $16.92 \pm 5.57 \text{ nm / minute}$ . These uncertainties in thickness represent real variations in thickness within the thin films. The AFM itself is accurate to within a nanometer. It was also found that slide placement plays a significant role in film thickness regardless of precursor ordering. The thickness of CTZ-2 was found to be  $710.2 \pm 162.0$ , which was comparable to many other slides, whereas CTZ-1 had the greatest film thickness by far (recall that the CTZ-1 and CTZ-2 films were created within the same deposition run, with the numbers indicating relative proximity to the precursor feed-throughs).

AFM was also used to calculate RMS roughness and percent roughness of the films (see Fig. 7 - 12). Scans were taken over 40x40 micrometer areas of unbroken thin film or 5x5 micrometer areas using higher resolution (either method should give comparable results for calculating roughness). From these, the RMS roughness and percent roughness of the films was calculated using the AFM software, Ambios. These results are also shown on Table 1. We see the RMS roughness was approximately 10% for most slides indicating a relatively rough surface, which is consistent for CVD.

## 3.2 Ultraviolet-visible-infrared Spectroscopy

Ultraviolet-visible-infrared spectroscopy (UV-Vis-IR) is a technique that measures the absorption of electromagnetic radiation by a sample as a function of wavelength. Determining the wavelengths that are most strongly absorbed by a thin film allows us to deduce information about the films valence and conduction bands and estimate the band gap of the film. The band gap is a particularly important piece of information for making solar cells. If radiation has a greater energy than the band gap of a solar cell, it can be absorbed, but the difference in energy is converted into heat instead of useful electrical energy [14]. Therefore, to maximize solar cell efficiency, it is important to precisely control the band gap of the solar cell.

To carry out UV-Vis-IR spectroscopy, a sample, in our case a thin-film, is exposed to a beam of electromagnetic radiation of a known energy range. The incident and transmitted intensities of the beam are recorded. The transmitted intensity ( $I_T$ ) is equal to the incident intensity ( $I_0$ ) multiplied by a decreasing exponential. The exponential is a function of film thickness and the absorption coefficient of the sample (which depends on the type of atoms in the sample and the energy of the incident radiation),

$$I_T = I_0 e^{-\mu(E)x}$$

Since ( $I_0$ ), ( $I_T$ ), and film thickness  $x$  are known, the absorption coefficient can easily be found.

With this, Tauc plots of  $(h\nu)^x$  vs.  $h\nu$  can be used to estimate the band gap of the films, where  $x = 1$  for direct band gaps and  $x = 2$  for indirect band gaps [15]. This is a standard method for determining the band gap in which a straight line is fit to the region of sharpest incline of the absorbance spectra and determine the x-axis intercept. The band gap energy is given by the x-axis intercept.

Tauc plots for the films, constructed from data taken at NASA Ames Research Laboratory, are shown in Figs. 13 - 18. The results are summarized on Table 2, which shows the direct band gaps to be approximately  $1.35 \pm 0.30$  eV for CTZ-1,  $1.63 \pm 0.20$  eV for CTZ-2,  $1.88 \pm 0.20$  eV for CZT-1,  $2.02 \pm 0.20$  eV for TCZ-1,  $1.56 \pm$

0.20 eV for TCZ-2, &  $1.08 \pm 0.20$  eV for ZTC-1. The band gap of CZTS has been reported to be 1.5 eV [5]. While these values are encouraging, Tauc plots provide only an estimation of the band gap and cannot be used to confirm whether or not the films are truly CZTS.

### 3.3 Energy-Dispersive X-Ray Spectroscopy

Energy-dispersive x-ray spectroscopy (EDX) is a technique similar to UV-Vis-IR except that it uses radiation in the x-ray region. EDX is useful for determining the stoichiometric ratios of elements present within a sample. During EDX measurements, the absorption of incident x-rays will greatly increase when the x-ray energy matches the binding energy of electron to an element present in the thin film. This causes a dramatic drop in transmitted x-ray intensity, known as an absorption edge. Because each element has a unique set of absorption edges, corresponding to the various binding energies of its electrons, it is possible to determine what elements are present in the sample. The relative height of the peaks allows the ratios of these elements to be determined. EDX data are typically shown as graphs of the absorption coefficient vs energy, beginning near the absorption edge of an element in the sample, usually in the 500 to 1000 eV range. EDX is performed in much the same way as UV-Vis-IR spectroscopy. A sample, in our case a thin-film, is exposed to x-rays of a known energy. The incident and transmitted intensities of the x-ray beam are recorded. This is done over a range of energies. Equation [1] again applies.

EDX was performed on the samples at NASA Ames Research Laboratory using 100-, 1000-, and 5000-times magnification. Data were collected for 240 seconds using 15.0 kV accelerating voltage. The results proved to be consistent regardless of magnification. Spectra for 1000x magnification are shown in Fig. 19 - 24. Tables 4-9 summarize the corresponding percent weights. Each spectrum shows the presence of copper, tin, and zinc as expected. From the relative height of the peaks, the element ratios were estimated. The ideal element ratios for CZTS are  $\text{Cu}/(\text{Zn}+\text{Sn}) = 0.9$

and  $\text{Zn}/\text{Sn} = 1.2$  [16]. Table 3 summarizes the ratios for our samples, showing that all ratios are quite far from the ideal. However, these ratios are not entirely reliable because we did not have a known sample of CZTS for comparison. It is possible that the detector is more sensitive to some energies than others. Thus, although the measurements reliably show which elements are present, without a known sample to calibrate with, we must be skeptical of the calculated ratios. When a known sample of CZTS is obtained, this data will be revisited.

### 3.4 X-Ray Diffraction

X-ray diffraction (XRD) is a phenomenon wherein the atomic and molecular structure of a substance cause a beam of x-rays to diffract into many specific angles. Because the diffraction pattern of any given substance is unique to the atoms and structure of that substance, the angles and intensities of the diffracted x-rays can be measured to produce a three-dimensional picture of the electron density within the substance. From this, the average position of atoms and the crystallinity of the substance can be determined. The compounds present within a substance can be determined by comparing its diffraction pattern to known diffraction patterns.

There are multiple techniques of varying sophistication which make use of x-ray diffraction (e.g., powder diffraction, Laue diffraction, etc.), but at the foundation of all of them is Bragg's Law,  $(2d)\sin\theta = n\lambda$ , where  $d$  is the spacing between diffracting planes,  $\theta$  is the incident angle,  $\lambda$  is the x-ray wavelength, and  $n$  is an integer. Incoming x-rays interact with electrons in the sample, producing spherical waves which emanate from the interacting electron. Crystalline structures have regular arrays of atoms which in turn produce regular arrays of spherical waves. In most directions, outgoing waves will partially or completely cancel each other out due to destructive interference. However, constructive interference will occur at angles dictated by Bragg's law.

For a typical XRD measurement, a sample is put on a goniometer (an instrument that allows the sample to be rotated by precise angles) and incrementally rotated as it is bombarded with x-rays of known energy. Fourier transforms can be used to create a three-dimensional model of the density of electrons within the sample using the two-dimensional diffraction pattern images taken at various angles.

For each of the slides, XRD measurements were performed at UCSC using continuous scan mode with a rate of 3.0000 deg/min, 0.0100 degree step-size, over a range of 20 to 80 degrees. The incident slit of the apparatus was 1.000 mm and the receiving slit was 10.000 mm. The diffraction patterns for the slides are shown in Figs. 25-29. Strangely, no pattern at all was observed for ZTC-1 despite repeated attempts. For all other slides, we see the diffraction pattern has a considerable amount of background noise, peak broadening, and peak shifting. Some amount of noise is to be expected because of how thin the films are relative to the substrate. Normally, an XRD measurement of samples such as ours would show a tall, sharp quartz diffraction peaks which would be much stronger than the peaks we are interested in. Suppressing the quartz pattern (using software) amplifies the peaks we are interested in as well as the noise. However, more interestingly, the level of noise present in these patterns also indicates that the films have low crystallinity. Crystallinity refers to how much long-range order a substance has. For example, amorphous glass has very short-range order. Its XRD spectra would look very noisy and spread out. An infinite crystal would have long-range order and its XRD spectra would show tall, sharp peaks with very low noise. Given that these films were produced with CVD, it is not too surprising that they are amorphous.

Peak shifting occurs when one compound has some of its atoms replaced by atoms which bond in a similar manner. For example, Cu<sub>2</sub>S and ZnS have similar bonding structures and pure samples of each have XRD spectra with peaks that are near one another. With broad, noisy peaks such as the ones we see from our samples, and given the fact that we used multiple precursors, it is very difficult to tell if a given

peak is just broadened, shifted and broadened, or two peaks blurred together.

Given these difficulties with identification, the results do not confirm or disprove that the samples are CZTS. However, the results are suggestive. There are at least three peaks that appear to correspond what we would expect to be present if CZTS were formed (compare Fig. 39 to Figs. 25 - 29). Specifically, there appears to be a large peak at 30 degrees which corresponds to the (1 1 2) plane of CZTS [17]. There are also peaks that could suggest formation of metal-sulfides. For TCZ-1, we see peaks that correspond to zinc sulfide, ZnS, (1 1 1), (2 0 0), (2 2 0), and (3 1 1) (based on comparison with DB card number 01-077-3378). For TCZ-2, we see peaks possibly corresponding to copper sulfide Cu<sub>1.8</sub>S (1 1 1), (2 0 0), (2 2 0), (3 1 1) and tin sulfide SnS<sub>2</sub> (1 0 1), (0 0 18), (1 1 0) and (1 1 18), (DB card numbers 01-070-9132 and 00-040-1466, respectively). For CZT1-, tin sulfide SnS (1 1 1), (2 0 0), and (2 2 0) (DB card number 01-077-3356). CTZ-1 showed zinc sulfide ZnS (1 1 1), (2 2 0) and (3 1 1) while CTZ-2 showed possible matches with copper sulfide Cu<sub>1.8</sub>S (1 1 1), (2 0 0), (2 2 0), and (3 1 1).

Overall, the XRD results indicate that the films have low crystallinity and, while the formation of CZTS could not be confirmed with this technique, the results are encouraging in that they suggest the presence of peaks we expected to see. In the future, it possible that better XRD results would be obtained by using a slower scan rate. This would allow more data to be collected, with the likely result that the increased signal from peaks would outpace the noise thereby revealing peaks that were buried amidst the noise in these results.

### 3.5 Four-Point Resistivity

The resistivity of a thin film is a basic property useful for determining its electrical characteristics. It can also give clues as to how successful complete a deposition was. For example, if the resistance measurement indicates an infinite resistance then it is

likely that the deposition is not continuous.

Normally resistance is measured with a simple, two-pronged ohmmeter. However, the resistance of the cables of a simple ohmmeter can cause problems with the measurement when the contact area is very small, as it is with thin films. A better alternative is to take a 4-point resistivity measurement. As the name implies, this is done with four probes; a current is passed through the outer two and the voltage is measured using the inner two. This effectively creates the circuit shown in Figure 31, where  $R_{Ci}$  is the resistance due to contact  $i$ ,  $R_S$  is the resistance of the sample,  $R_M$  is the equivalent resistance of the voltmeter,  $V_S$  is the voltage across the sample, and  $V_M$  is the voltage measured using the voltmeter.

Table 10 includes the 4-point resistivity measurements of the samples. The high resistance values observed are desirable because they indicate that the films may behave like semiconductors rather than conductors. Despite wanting a relatively high resistance, an overflow (as observed with ZTC-1) is somewhat undesirable because, as previously mentioned, it can indicate that the film is discontinuous. For a solar cell to work, the mobility of the film must be high enough that electron-hole pairs can get out of the film and into metal interfaces. A discontinuous film would therefore be problematic.

## Chapter 4

# Discussion

In this experiment, the effect of stacked precursor ordering on CZTS thin films was examined. Similar research has been done, notably by Hiroshi Nozaki et al. [6] and Seung Shin et al. [17], both of whom examined the same precursor orderings as were examined in this experiment. The main difference between the experiments are that both Nozaki and Shin used a sputtering method for depositions, whereas we used CVD. Sputtering is considered a physical deposition method, as opposed to chemical. Molecules are ejected from a target (such as a block of zinc sulfide, for example) by means of violent collisions with inert gas. Ejected molecules coat a substrate. A detailed discussion of the relative pros and cons of each method would lead this paper astray. Briefly, sputtering has the advantage that pure metal can be used rather than potentially toxic metal-organic precursors. However, determining precursors that will work for CVD is proof-of-concept for ALD, a method of deposition that produces extremely conformal films because the reaction is self-limiting, allowing just a single layer to be created at a time (CVD was used in this experiment because it is less time-consuming). ALD is also more easily scaled than sputtering, which would be useful for industrial scale production of thin films. Shin found band gap energies between 1.10 and 1.45 eV, a smaller range than our films. Nozaki did not report band gap energies. Both shin and nozaki determined the CZTS they created to have a kesterite structure. Our XRD results were too noisy to determine the molecular structure of our thin films. Another analysis technique, extended x-

ray absorption fine structure (EXAFS), could give us the answer. At the time of this writing, EXAFS have been performed on our thin-films but results are pending. Whether or not the deposition method significantly affects the efficiency of CZTS thin-film solar films remains to be seen. In this paper, merely another method of creating CZTS has been examined. If further research using this method proves viable for creating thin-film solar cells, this method may have an advantage over the sputtering method of deposition in that it is more easily scaled.

## Chapter 5

# Conclusion

CZTS thin-films show promise for the development of cheap, non-toxic, high-efficiency thin film photovoltaics. Layered thin films were created with copper, tin, and zinc precursors using CVD and then annealed in hydrogen sulfide, in the hopes of producing CZTS thin films. Four different precursor stacking sequences were examined: CTZ, CZT, TCZ, and ZTC. It was found that the sequence of precursors has a significant effect on the resulting thin film. It was also found that the proximity of the substrate to the precursor feedthroughs significantly affected the resulting stoichiometry of the thin film. As is common with CVD, the thicknesses of the films were found to vary considerably. Among the slides, thickness was found to range from as thin as approximately 250 nm for CZT-2 to as much as 893 nm for CTZ-1, corresponding to growth rates of 2.77 nm/min. and 9.33 nm/min., respectively. For individual slides, thickness was found to differ as much as 200 nm across the scan area (CZT-1) or as little as 40 nm (TCZ-2). The percent roughness for the slides was found to be consistent with CVD. Direct band gaps for the films suggest that the combinations CTZ and TCZ are viable for creating CZTS. However, film properties were found to vary considerably based on substrate placement. For example, the band gap for TCZ-2 was found to be 1.56 eV, very near the literature value of 1.5 eV, yet the band gap for TCZ-1 was found to be 2.02 eV. This suggests that this ordering of precursors should be further examined for reproducibility, with attention paid to slide placement. X-ray diffraction results show that the films were highly

amorphous. This, combined with the level of noise due to how thin the films were, prevented XRD from confirming whether or not the films were CZTS. However, the results were suggestive in that there were XRD peaks appeared to correspond to CZTS, most notably the (1 1 2) plane of CZTS at 30 degrees. A previously untested tin precursor, Dibutyltin Diacetate, was used in this experiment. The results suggest that this precursor is viable for creating CZTS. Further experiments should be done to test the reproducibility of these results. Though this is true for any experiment, the way the results varied depending upon substrate placement within the tube furnace and the goal of reliably producing CZTS thin film on an industrial scale make reproducibility an important question. In this experiment, all precursors were deposited by 30 minute CVD. Varying these times would change the properties of the resulting films; optimization of the deposition times may very well lead to a method consistently produce CZTS and should thus be investigated as well. Additionally, two remaining precursor orderings remain to be tested: TZC and ZCT. Based on the results of this experiment, future analysis of thin films using XRD should be done at a scan rate of less than 3 degrees/minute to improve the signal to noise ratio.

## 5.1 Test Figure/Table

Below are a test figure and a test table to show usage, and that they actually populate the automatically generated lists at the beginning of the document.

# Appendices

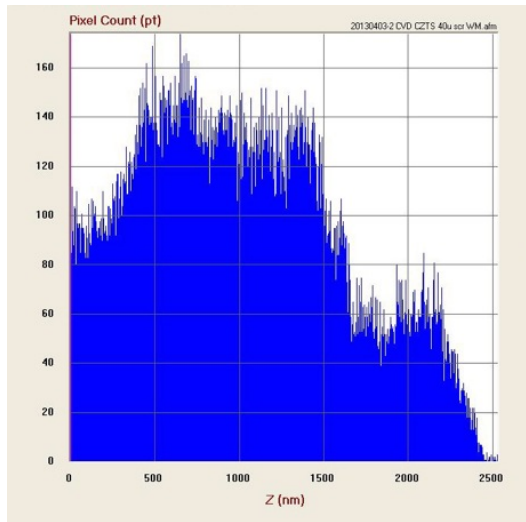


Figure 1: Step-height histogram for AFM scan of scratched CTZ-1 film.

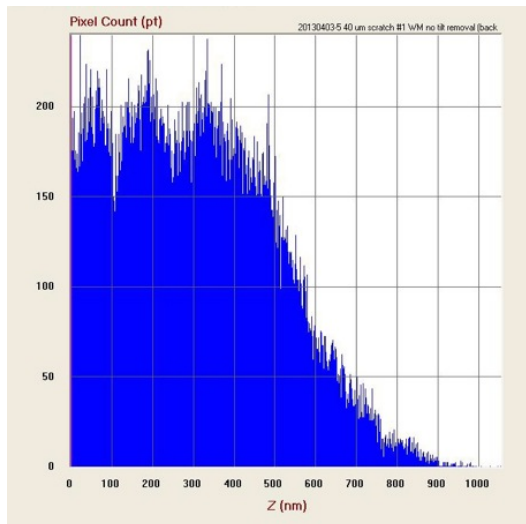


Figure 2: Step-height histogram for AFM scan of scratched CTZ-2 film.

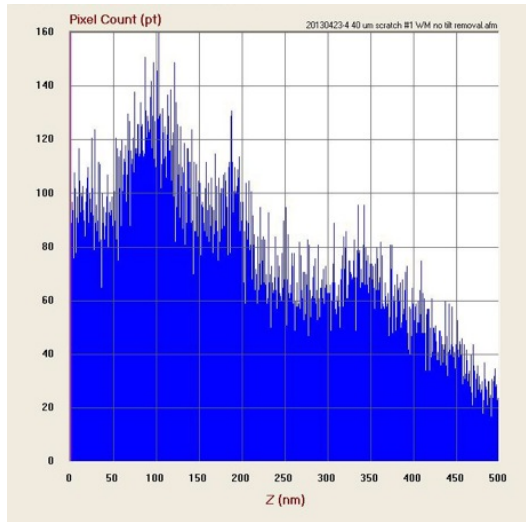


Figure 3: Step-height histogram for AFM scan of scratched ZTC-1 film.

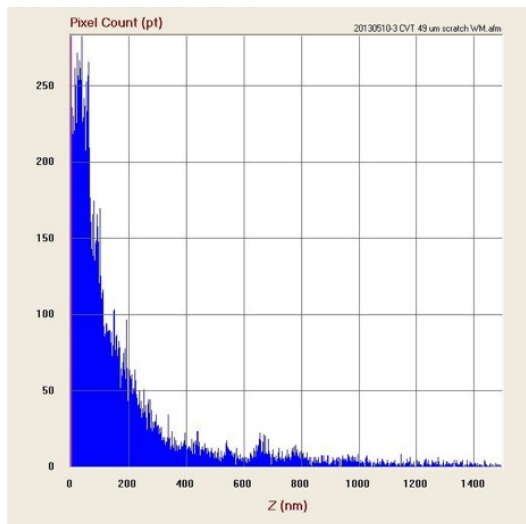


Figure 4: Step-height histogram for AFM scan of scratched TCZ-1 film.

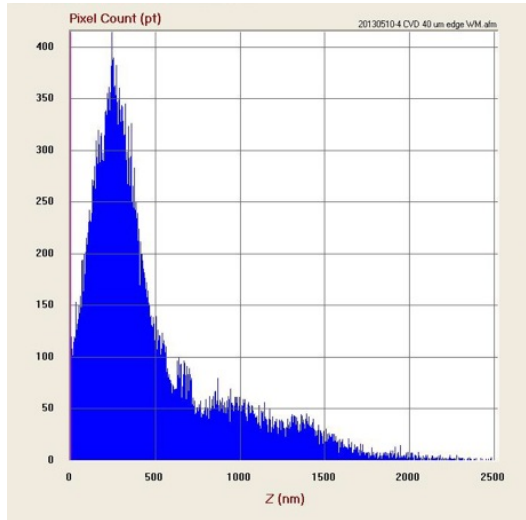


Figure 5: Step-height histogram for AFM scan of scratched TCZ-2 film.

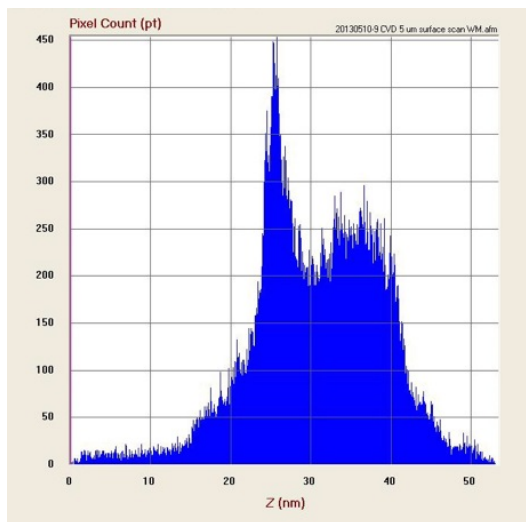


Figure 6: Step-height histogram for AFM scan of scratched CZT-1 film.

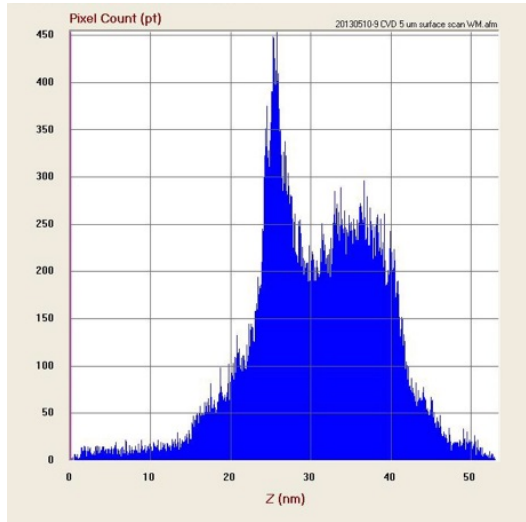


Figure 7: Relative height histogram for surface scan of CTZ-1.

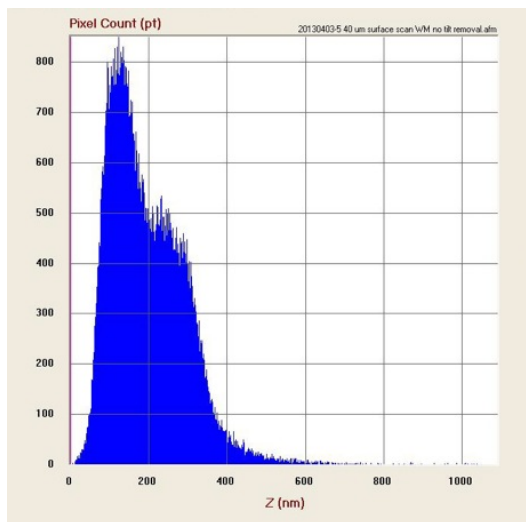


Figure 8: Relative height histogram for AFM surface scan of CTZ-2.

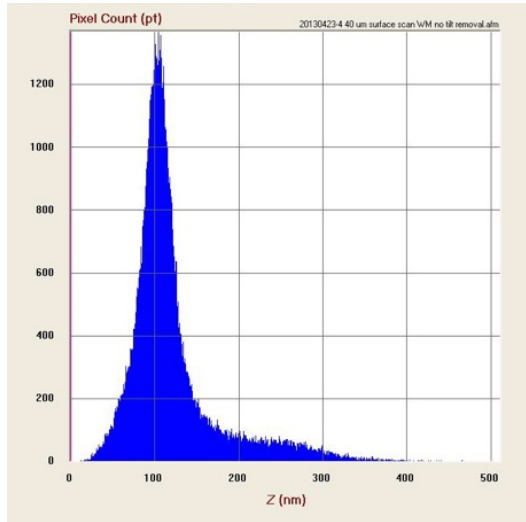


Figure 9: Relative height histogram for AFM surface scan of ZTC-1.

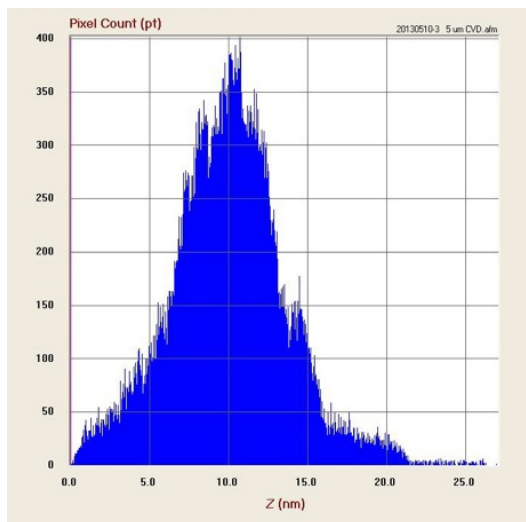


Figure 10: Relative height histogram for AFM surface scan of TCZ-1.

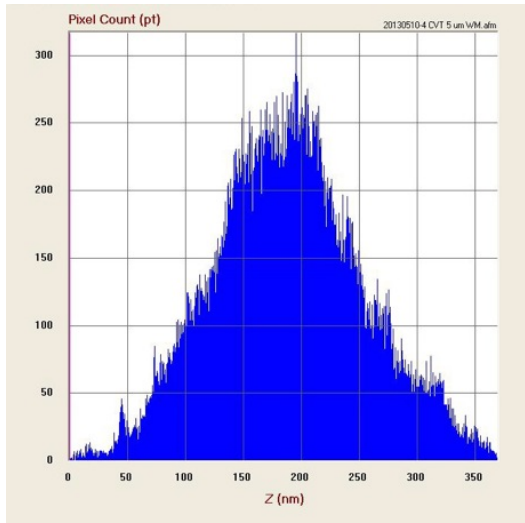


Figure 11: Relative height histogram for AFM surface scan of TCZ-2.

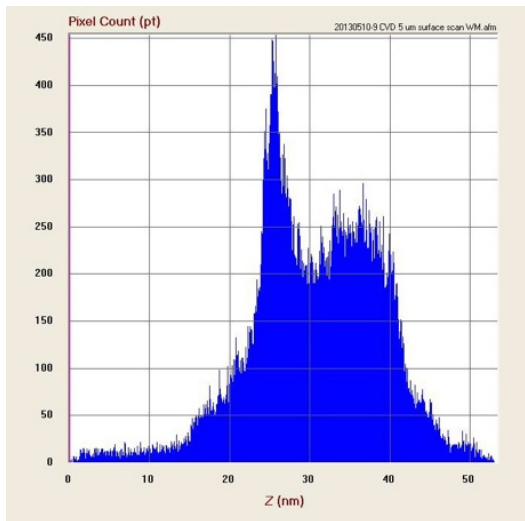


Figure 12: Relative height histogram for AFM surface scan of CZT-1.

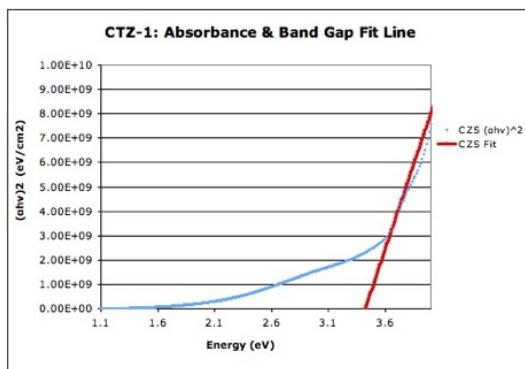


Figure 13: Tauc plot for CTZ-1. The fit line intercepts the x-axis at 3.40 eV.

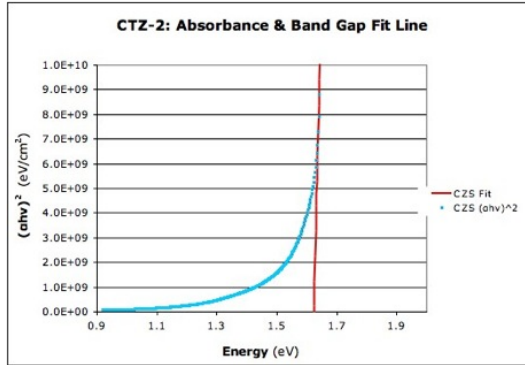


Figure 14: Tauc plot for CTZ-2. The fit line intercepts the x-axis at 1.63 eV.

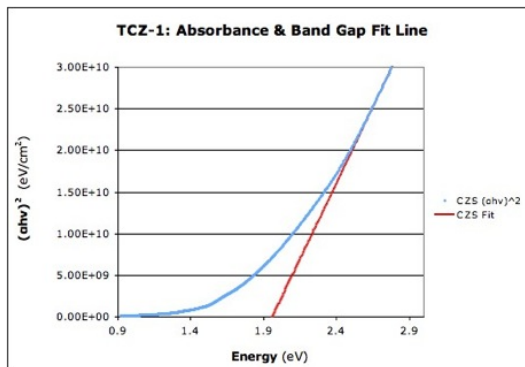


Figure 15: Tauc plot for TCZ-1. The fit line intercepts the x-axis at 2.02 eV.

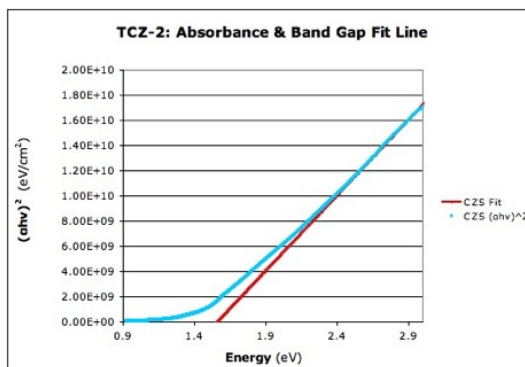


Figure 16: Tauc plot for TCZ-2. The fit line intercepts the x-axis at 2.39 eV.

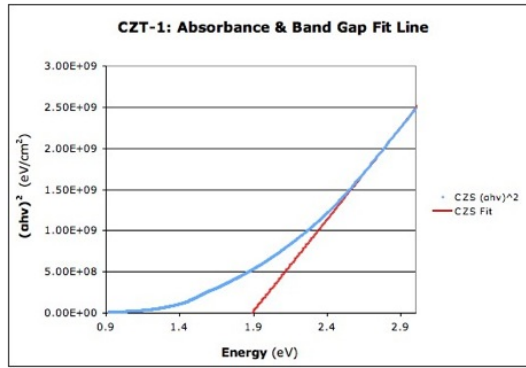


Figure 17: Tauc plot for CZT-1. The fit line intercepts the x-axis at 1.87 eV.

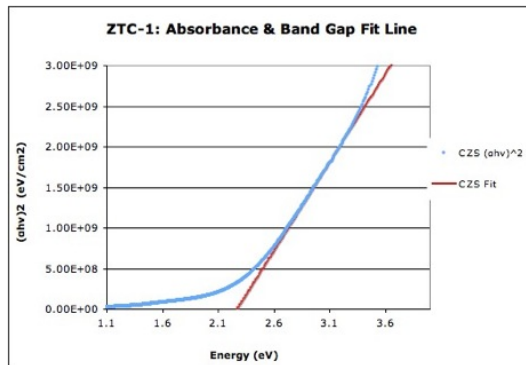


Figure 18: Tauc plot for ZTC-1. The fit line intercepts the x-axis at 1.08 eV.

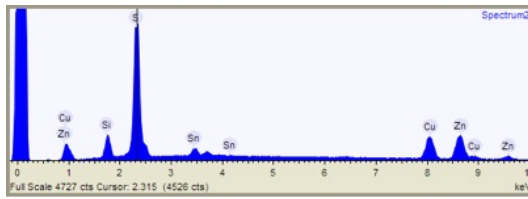


Figure 19: EDX spectrum for CTZ-1 at 1000X magnification.

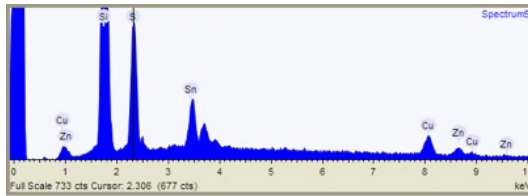


Figure 20: EDX spectrum for CTZ-2 at 1000X magnification.

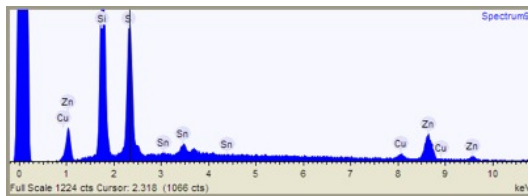


Figure 21: EDX spectrum for ZTC-1 at 1000X magnification.

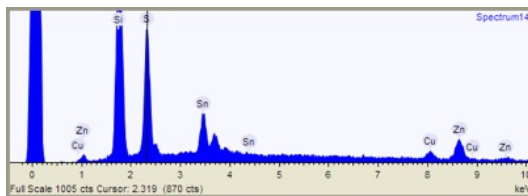


Figure 22: EDX spectrum for TCZ-1 at 1000X magnification.

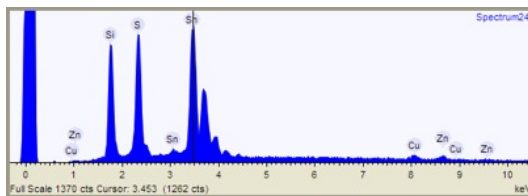


Figure 23: EDX spectrum for TCZ-2 at 1000X magnification.

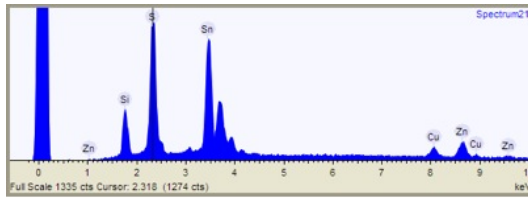


Figure 24: EDX spectrum for CZT-1 at 1000X magnification.

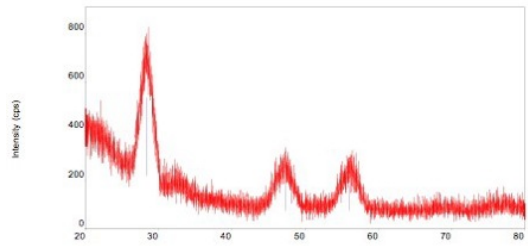


Figure 25: X-ray diffraction pattern for CTZ-1 showing intensity (y-axis) versus diffraction angle (x-axis).

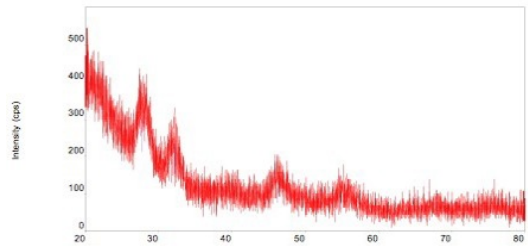


Figure 26: X-ray diffraction pattern for CTZ-2.

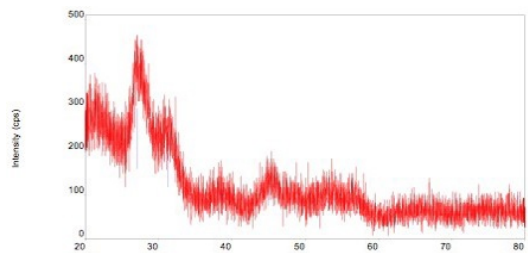


Figure 27: X-ray diffraction pattern for CZT-1.

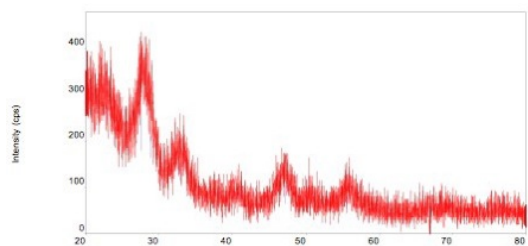


Figure 28: X-ray diffraction pattern for TCZ-1.

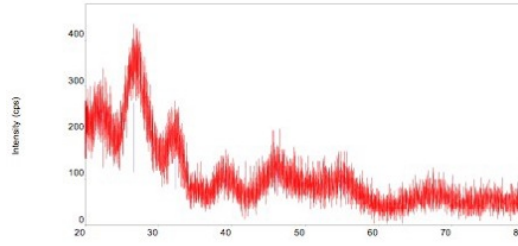


Figure 29: X-ray diffraction pattern for TCZ-2.

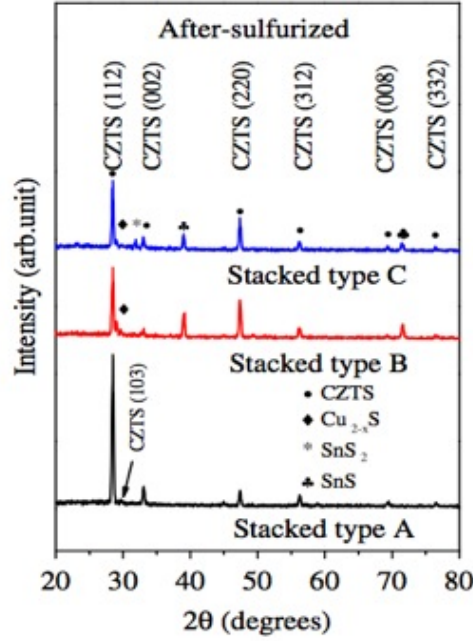


Figure 30: Reference XRD pattern for three different stacking orders of CZTS. Stacked type A corresponds to CTZ, B to ZCT, and C to TZC. (This image is taken from reference 17)

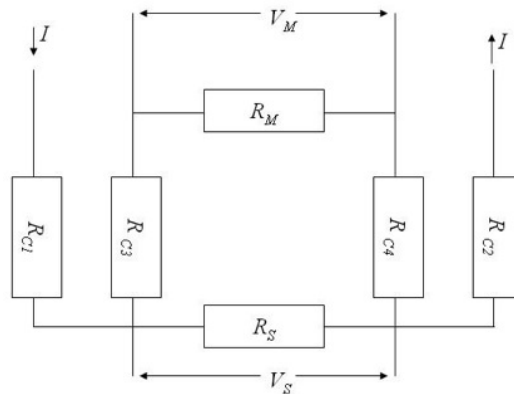


Figure 31: Effective circuit for 4-point resistivity measurement.  $R_{Ci}$  is the resistance due to contact  $i$ ,  $R_S$  is the resistance of the sample,  $R_M$  is the equivalent resistance of the voltmeter,  $V_S$  is the voltage across the sample, and  $V_M$  is the voltage measured using the voltmeter.

Table 1: Atomic Force Microscopy Data

Deposition Layering	Film Thickness (nm)	Growth Rate (nm/min)
CTZ-1	1523.0 $\pm$ 501.3	16.92 $\pm$ 5.57
CTZ-2	710.2 $\pm$ 162.0	7.89 $\pm$ 1.80
ZTC-1	704.4 $\pm$ 113.9	7.82 $\pm$ 1.27
TCZ-1	710.0 $\pm$ 192.4	7.88 $\pm$ 2.13
TCZ-2	997.5 $\pm$ 328.7	11.08 $\pm$ 3.65
CZT-1	1033.1 $\pm$ 155.5	11.48 $\pm$ 1.73

Table 2: Direct Band Gaps

Deposition Layering	Direct Band Gap (eV)
CTZ-1	1.35 $\pm$ 0.30
CTZ-2	1.63 $\pm$ 0.20
ZTC-1	1.08 $\pm$ 0.20
TCZ-1	2.02 $\pm$ 0.20
TCZ-2	1.56 $\pm$ 0.20
CZT-1	1.88 $\pm$ 0.20

Table 3: Stoichiometric Ratios

Deposition Layering	Cu/(Zn+Sn) Ratio	Zn/Sn Ratio
CTZ-1	0.567	1.049
CTZ-2	0.278	0.246
ZTC-1	0.004	0.005
TCZ-1	0.117	0.262
TCZ-2	0.026	0.052
CZT-1	0.137	3.150

Table 4: Summary results of EDX spectrum for CTZ-1 at 1000X magnification

Element	Percent Weight
Silicon	8.5
Sulfur	49.0
Copper	20.2
Zinc	11.7
Tin	10.7

Table 5: Summary results of EDX spectrum for CTZ-2 at 1000X magnification

Element	Percent Weight
Silicon	50.7
Sulfur	21.6
Copper	4.9
Zinc	3.0
Tin	19.7

Table 6: Summary results of EDX spectrum for ZTC-1 at 1000X magnification

Element	Percent Weight
Silicon	39.3
Sulfur	35.4
Copper	2.0
Zinc	15.7
Tin	7.5

Table 7: Summary results of EDX spectrum for TCZ-1 at 1000X magnification

Element	Percent Weight
Silicon	42.7
Sulfur	27.4
Copper	1.2
Zinc	4.0
Tin	24.7

Table 8: Summary results of EDX spectrum for TCZ-2 at 1000X magnification

Element	Percent Weight
Silicon	17.8
Sulfur	19.3
Copper	0.8
Zinc	1.5
Tin	60.7

Table 9: Summary results of EDX spectrum for CZT-1 at 1000X magnification

Element	Percent Weight
Silicon	9.0
Sulfur	26.1
Copper	0.0
Zinc	0.0
Tin	64.9

Table 10: Four-Point Resistivity Measurements

Deposition Layering	Four-Point Resistance (M $\Omega$ m)
CTZ-1	22.0 $\pm$ 0.5
CTZ-2	25.0 $\pm$ 0.5
ZTC-1	overflow
TCZ-1	30.0 $\pm$ 0.5
TCZ-2	0.50 $\pm$ 0.05
CZT-1	100. $\pm$ 1

# Bibliography

- [1] Global Business Intelligence Research, Thin-Film Photovoltaic (PV) Cells Market Analysis to 2020 - CIGS (Copper Indium Gallium Diselenide) to Emerge as the Major Technology by 2020, (June 2010)
- [2] Critical Reviews in Solid State and Materials Sciences, Copper Indium Selenides and Related Materials for Photovoltaic Devices, Volume 27, Issue 2, (2002)
- [3] Repins, I., Contreras, M. A., Egaas, B., DeHart, C., Scharf, J., Perkins, C. L., To, B. and Noufi, R. (2008), 199
- [4] Cyrus Wadia, A. Paul Alivisatos and Daniel M. Kammen , Materials Availability Expands the Opportunity for Large-Scale Photovoltaics Deployment Environ. Sci. Technol., 2009, 43 (6), pp 20722077
- [5] H. Katagiri, Cu<sub>2</sub>ZnSnS<sub>4</sub> thin film solar cells, Thin Solid Films 480481 (2005) 426432.
- [6] Hiroshi Nozakia, Tatsuo Fukanoa, Shingo Ohtaa, Yoshiki Senoa, Hironori Katagirib, Kazuo Jimbob, Crystal structure determination of solar cell materials: Cu<sub>2</sub>ZnSnS<sub>4</sub> thin films using X-ray anomalous dispersion, Journal of Alloys and Compounds 524 (2012) 2225
- [7] T.K. Todorov, K.B. Reuter, D.B. Mitzi, High-efficiency solar cell with Earth- abundant liquid-processed absorber, Adv. Mater. 22 (2010) E156E159
- [8] W. Shockley, H.J. Queisser, Detailed balance limit of efficiency of pn junction solar cells, J. Appl. Phys. 32 (1961) 510512
- [9] J.J. Scragg, D.M. Berg, P.J. Dale, A 3.2 percent efficient Kesterite device from electro-deposited stacked elemental layers, J. Electroanal. Chem. 646 (2010) 5255

- [10] H. Araki, A. Mikaduki, Y. Kubo, T. Sato, K. Jimbo, W.S. Maw, H. Katagiri, M. Yamazaki, K. Oishi, A. Takeuchi, Preparation of Cu<sub>2</sub>ZnSnS<sub>4</sub> thin films by sulfurization of stacked metallic layers, *Thin Solid Films* 517 (2008) 14571460
- [11] H. Yoo, J.H. Kim, Growth of Cu<sub>2</sub>ZnSnS<sub>4</sub> thin films using sulfurization of stacked metallic films, *Thin Solid Films* 518 (2010) 65676572
- [12] Short et al., Atomic Layer Deposition of Zinc Sulfide with Zn(TMHD)<sub>2</sub>, *J. Vac. Sci. Technol. A* 31, 01A138 (2013)
- [13] Alannah Myers, On Atomic Layer Deposition: Tin Sulfide for Photovoltaic Devices, A thesis submitted to Department of Physic, University of California Santa Cruz, June 6, 2013
- [14] Jeremy Wade, An Investigation of TiO<sub>2</sub>-ZnFe<sub>2</sub>O<sub>4</sub> Nanocomposites for Visible Light Photo catalysis, A thesis submitted to Department of Electrical Engineering; College of Engineering, University of South Florida, March 24, 2005.
- [15] Z. Chen, T. Jaramillo, T. Deutsch, A. Kleiman-Shwarscstein, A. Forman, N. Gaillard, R. Garland, K. Takanabe, C. Heske, M. Sunkara, E. McFarland, K. Domen, E. Miller, J. Turner, H. Dinh, *J. Mater. Res.* 25, 3 (2010)
- [16] David B. Mitzi, Oki Gunawan, Teodor K. Todorov, Kejia Wang, Supratik Guha, The path towards a high-performance solution-processed kesterite solar cell, *Solar Energy Materials & Solar Cells* 95 (2011) 14211436
- [17] Seung Wook Shin, Jin Hyeok Kimb, S.M. Pawar, Jeong Yong Lee, Chan Young Park, Jae Ho Yun, Jong-Ha Moon, Studies on Cu<sub>2</sub>ZnSnS<sub>4</sub> (CZTS) absorber layer using different stacking orders in precursor thin lms, *Solar Energy Materials & Solar Cells* 95 (2011) 32023206
- [18] Four-point resistivity Figure from: <http://lamp.tugraz.ac.at/hadley/sem/4pt/4pt.php>